Supporting Information

Physicochemical Characterization of Diacyltetrol-Based Lipids consisting of both Diacylglycerol and Phospholipid headgroups

Narsimha Mamidi[a,†], *Sukhamoy Gorai*[a,†], *Bolledu Ravi*[b] *and Debasis Manna*[a,*]

[a]Department of Chemistry, Indian Institute of Technology Guwahati, Assam 781039, India

[b]Department of Chemical Engineering, Indian Institute of Technology Guwahati, Assam 781039, India

Table of Content

Table S2: Characteristic monolayer forming properties of the hybrid lipids at air-water interface.

lipid	Acyl chain length	A_0(Å^2)	$C_s^{-1}{}_{max}$ (mN/ m)	π_{comp} (mN/ m)
DAT-PA_{16}	16:16	66.2 ± 2.7	54.8 ± 1.9	25.2 ± 1.5
DAT-PA_{18}	18:18	86.4 ± 3.3	91.9 ± 4.4	33.1 ± 1.8
DAT-PS_{16}	16:16	70.1 ± 1.4	60.0 ± 1.7	47.3 ± 2.4
DAT-PS_{18}	18:18	90.3 ± 3.2	84.6 ± 3.4	35.1 ± 2.5
DAT-PG_{16}	16:16	88.6 ± 6.1	74.9 ± 3.1	41.5 ± 2.2
DAT-PG_{18}	18:18	124.8 ± 4.1	66.8 ± 3.5	28.9 ± 2.4

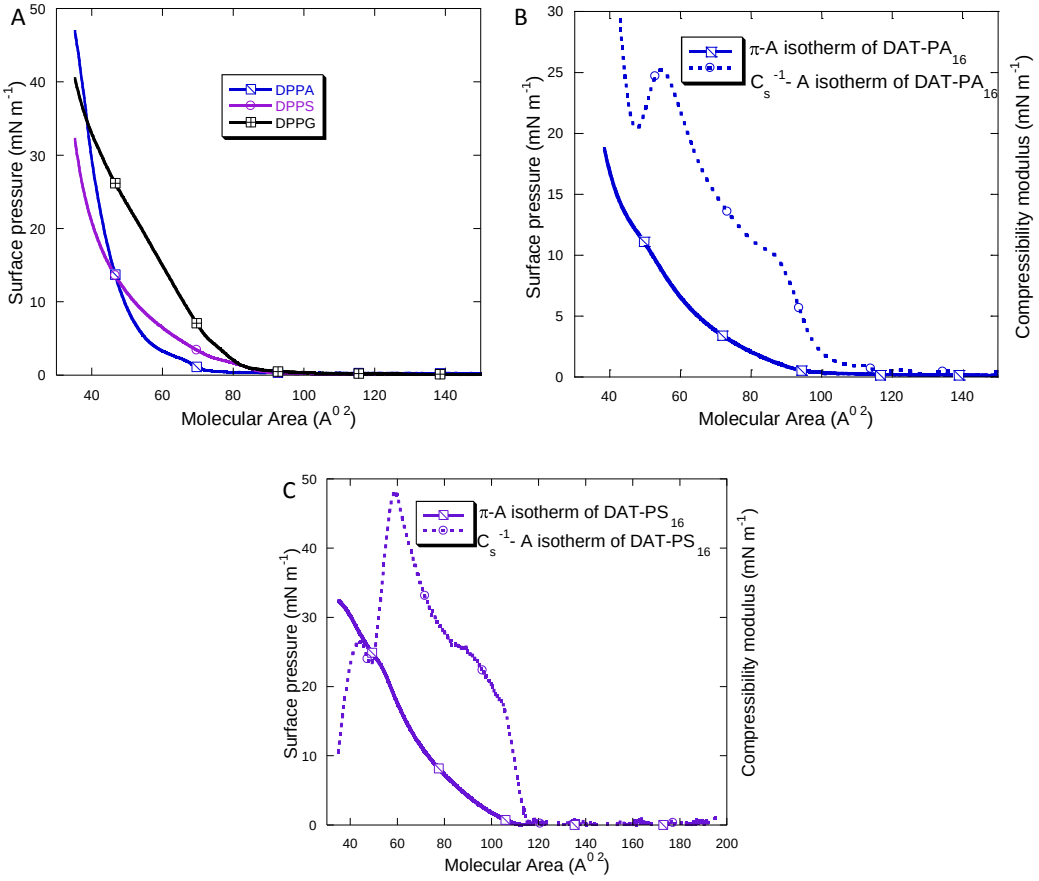

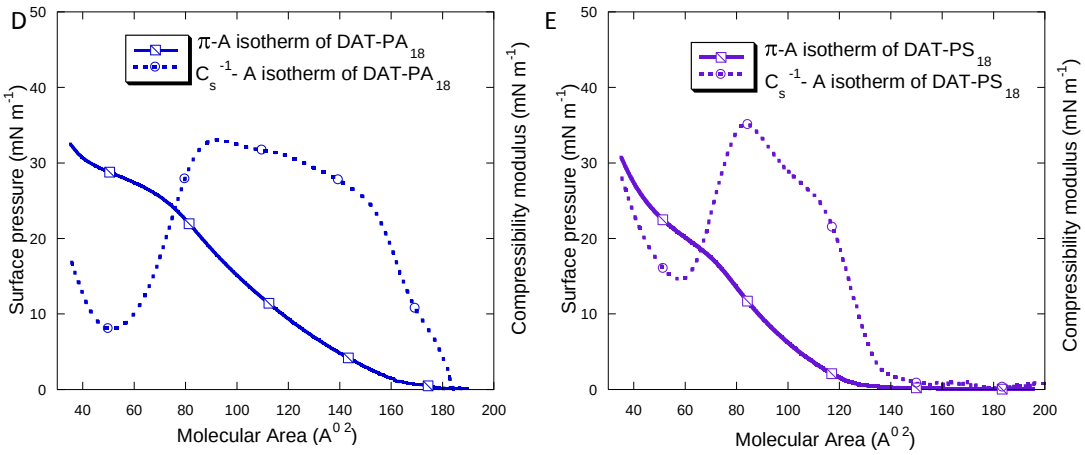

Figure S36: Air-water interfacial behavior of the lipids. (A) Surface pressure-molecular area (π-A) isotherm of DPPA (—), DPPS (—), and DPPG (—) lipids. (B) π-A (—) and compressibility moduluous (C_s^{-1})-A (▪▪▪) isotherms of DAT-PA_{16}. (C) π-A (—) and C_s^{-1}-A (▪▪▪) isotherms of DAT-PS_{16}. (D) π-A (—) and C_s^{-1}-A (▪▪▪) isotherms of DAT-PA_{18}. (E) π-A (—) and C_s^{-1}-A (▪▪▪) isotherms of DAT-PS_{18}. (E)

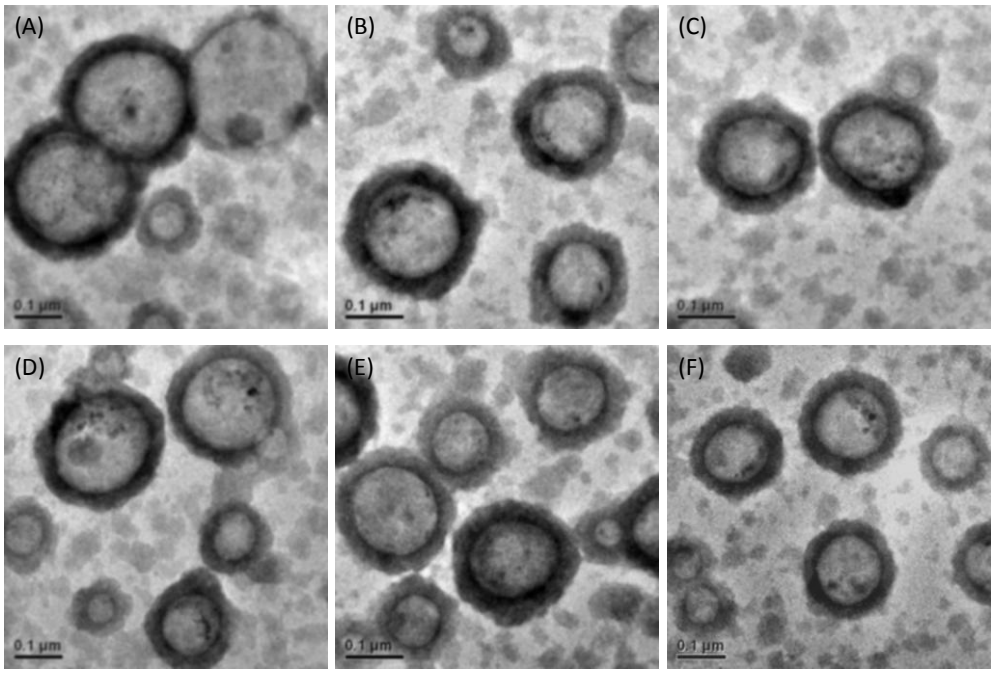

Figure S37: Representative TEM images of hybrid lipids in presence of cholesterol (hybrid lipids: Cholesterol (6:4)). TEM samples were prepared by negative staining with 1% uranyl acetate: (A) DAT-PA_{16}/Cholesterol liposomes, (B) DAT-PS_{16}/Cholesterol liposomes, (C) DAT-PG_{16}/Cholesterol liposomes, (D) DAT-PA_{18}/Cholesterol liposomes, (E) DAT-PS_{18}/Cholesterol liposomes, and (F) DAT-PG_{18}/Cholesterol liposomes.

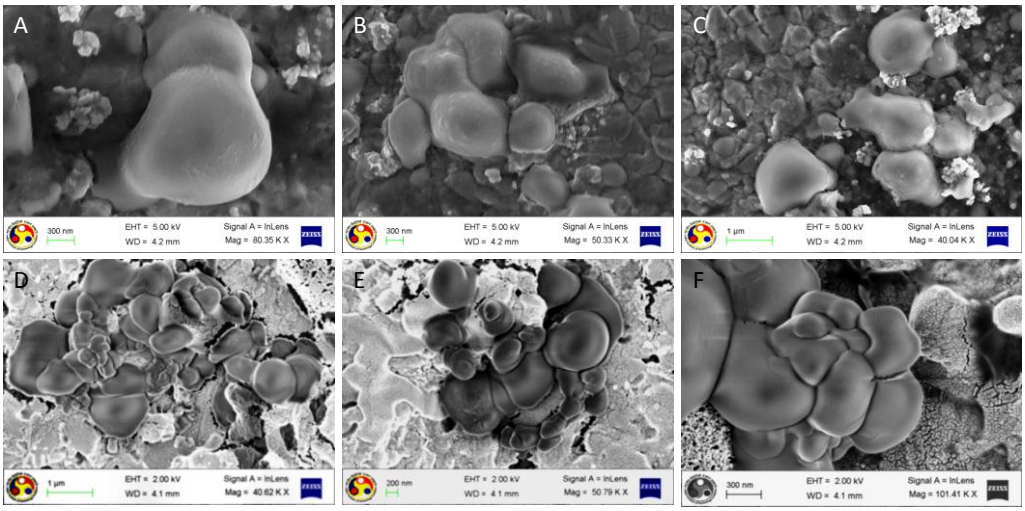

Figure S38: Representative FE-SEM images of hybrid lipids in presence of cholesterol (hybrid lipids: Cholesterol (6:4)): (A) DAT-PA_{16}/Cholesterol liposomes, (B) DAT-PS_{16}/Cholesterol liposomes, (C) DAT-PG_{16}/Cholesterol liposomes, (D) DAT-PA_{18}/Cholesterol liposomes, (E) DAT-PS_{18}/Cholesterol liposomes, and (F) DAT-PG_{18}/Cholesterol liposomes.

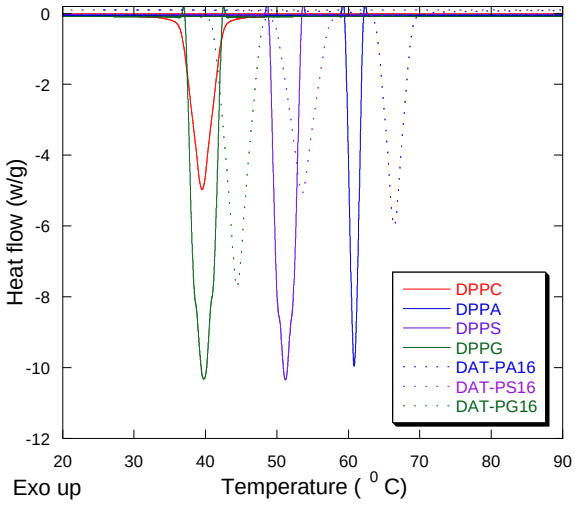

Figure S39: Differential scanning calorimetry study of liposomes.

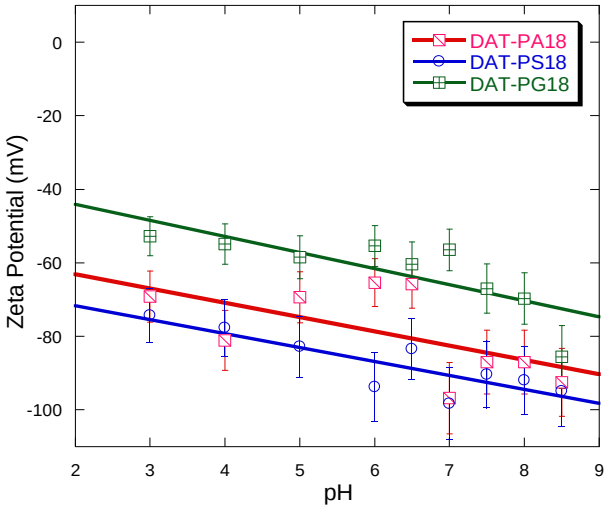

Figure S40: Zeta-potential of unsaturated hybrid lipids, DAT-PX$_{18}$ as a function of pH.

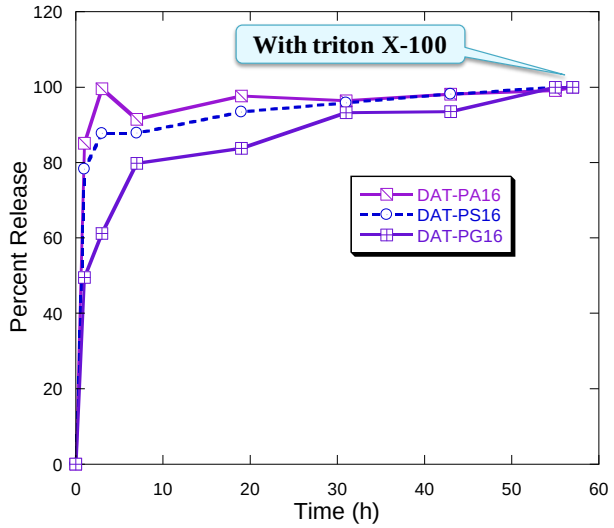

Figure S41: Rhodamine 6G (R6G) release profile from pure DAT-PX$_{16}$ liposomes.

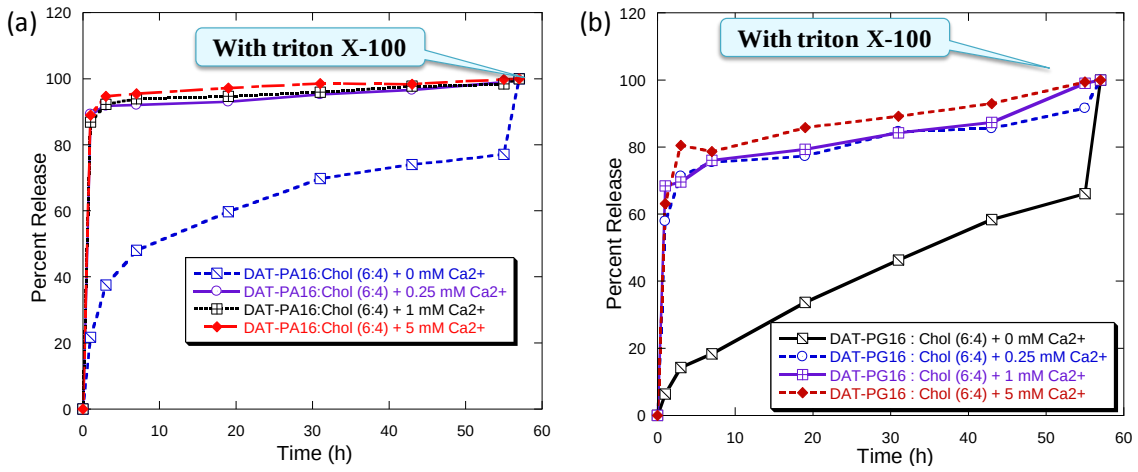

Figure S42: Rhodamine 6G (R6G) release profile from cholesterol containing DAT-PA_{16} and DAT-PG_{16} liposomes in absence and presence of different Ca^{2+} concentration.

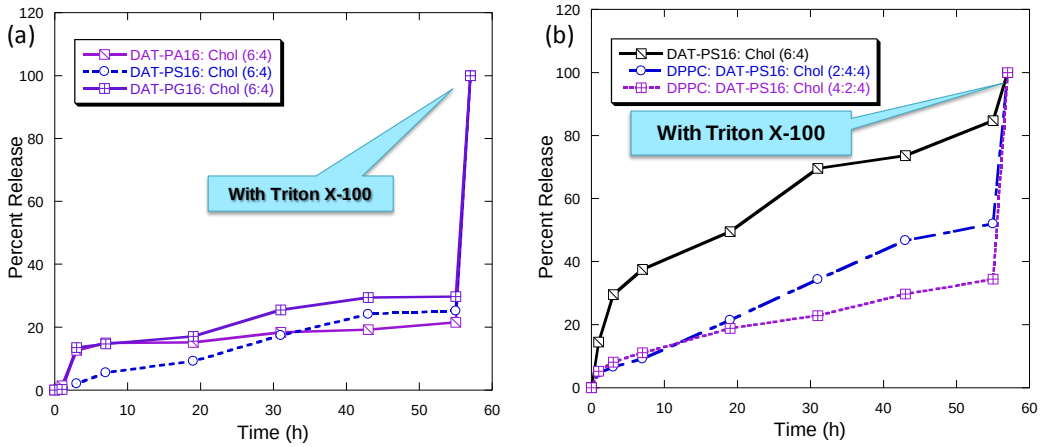

Figure S43: (a) Carboxyfluorescein (CF) release profile from cholesterol containing DAT-PX_{16} liposomes. (b) Rhodamine 6G (R6G) release profile from cholesterol containing DAT-PS_{16} and DPPC liposomes.

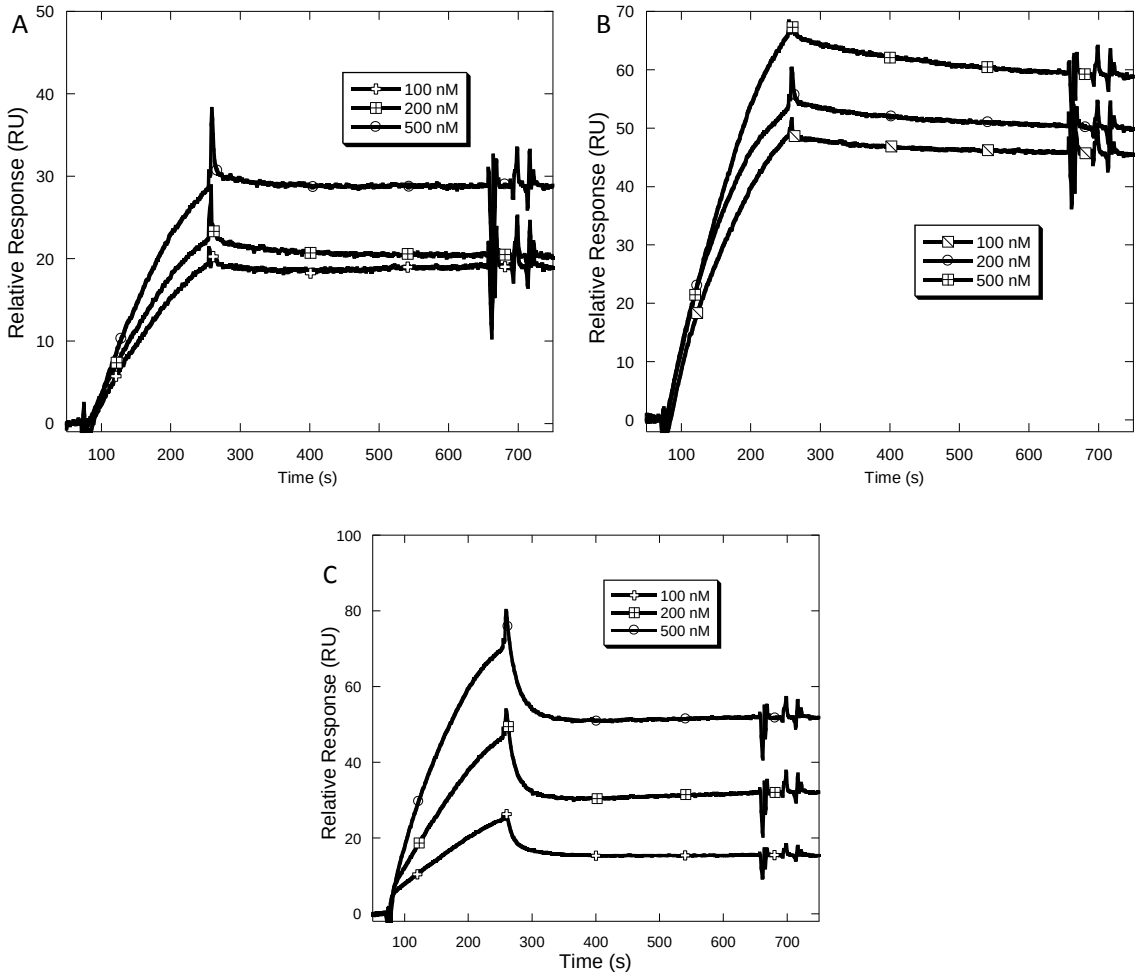

Figure S44: Kinetics of membrane binding of PKCθ-C1b subdomain. Kinetics of binding of PKCθ-C1b subdomain to the sensor chip coated with (A) PC/PE/DAT-PA_{16} (75/20/5), (B) PC/PE/DAT-PS_{16} (75/20/5) and (C) PC/PE/DAT-PG_{16} (75/20/5) vesicles. All sensorgrams were taken with the same concentration (100, 200, 500 nM) of PKCθ-C1b subdomain. Flow rate was kept at 30 μL/min. All the measurements were performed in 20 mM Tris, pH 7.4 containing 160 mM NaCl and 50 μM $ZnSO_4$.

Table S3. Membrane binding parameters of PKCθ-C1b subdomain determined from kinetics SPR analysis.

Values represent the mean ± S.D. from triplicate measurements. All the measurements were performed in 20 mM Tris, pH 7.4 containing 160 mM NaCl and 50 μM $ZnSO_4$.

Protein	PC/PE/DAT-PA_{16} (75:20:5)	PC/PE/DAT-PS_{16} (75:20:5)	PC/PE/DAT-PG_{16} (75:20:5)
PKCθ-C1b	6.4 ± 1.2 nM	13.6 ± 1.4 nM	19.1 ± 1.1 nM